

Ultralow Magnetic Damping in Co₂Mn-Based Heusler Compounds: Promising Materials for Spintronics

C. Guillemard,^{1,2} S. Petit-Watelot,¹ L. Pasquier,¹ D. Pierre,¹ J. Ghanbaja,¹ J-C. Rojas-Sánchez,¹ A. Bataille,³ J. Rault,² P. Le Fèvre,² F. Bertran,² and S. Andrieu^{1,*}

¹Institut Jean Lamour, UMR CNRS 7198, Université de Lorraine, 54506 Vandoeuvre lès Nancy, France

²Synchrotron SOLEIL-CNRS, L'Orme des Merisiers, Saint-Aubin, BP 48, 91192 Gif-sur-Yvette, France

³Laboratoire Léon Brillouin, IRAMIS, CEA Saclay, 91191 Gif-sur-Yvette, France



(Received 1 March 2019; revised manuscript received 30 April 2019; published 5 June 2019)

The prediction of ultralow magnetic damping in Co₂MnZ Heusler half-metal thin-film magnets is explored in this study and the damping response is shown to be linked to the underlying electronic properties. By substitution of the Z elements in high-crystalline-quality films (Co₂MnZ with Z = Si, Ge, Sn, Al, Ga, Sb), electronic properties such as the minority-spin band gap, Fermi-energy position in the band gap, and spin polarization can be tuned and the consequences for magnetization dynamics analyzed. The experimental results allow us to directly explore the interplay of spin polarization, spin gap, Fermi-energy position, and the magnetic damping obtained in these films, together with predictions from *ab initio* calculations. The ultralow magnetic damping coefficients measured in the range from 4.1×10^{-4} to 9×10^{-4} for Co₂MnSi, Co₂MnGe, Co₂MnSn, and Co₂MnSb are the lowest values obtained on a conductive layer and offer a clear experimental demonstration of theoretical predictions on half-metal magnetic Heusler compounds and a pathway for future materials design.

DOI: [10.1103/PhysRevApplied.11.064009](https://doi.org/10.1103/PhysRevApplied.11.064009)

I. INTRODUCTION

As a result of many theoretical and experimental advances, spintronic, electronics that use both the charge and spin of the electron, is progressing. Predictions of many phenomena, such as high-magnetoresistance MgO-based magnetic tunnel junctions [1,2], magnetization reversal by spin-transfer torques (STTs) [3,4], magnetization reversal by spin-orbit torques (SOTs) [5], and all-optical switching (AOS) by direct laser excitation [6], offer possibilities to design magnetoresistive random-access memories, magnetic sensors, and novel logic devices. Even more, the search for systems with high conversion efficiency of charge to spin or spin to charge current [7] are being explored for fundamental understanding of spin transport and for applications in low-energy-consumption devices. Most spintronic devices consist of thin-film heterostructures where interesting physics emerges at the interfaces [8]. For continued progress, magnetic materials with specific and dedicated properties are needed, such as a high Curie temperature and an appropriate magnetic anisotropy for thermal stability [9], a high spin polarization (SP) at the Fermi energy to obtain fully-spin-polarized currents, and a small magnetic damping to easily generate magnetization precession. All of these properties are desirable for STT-, SOT-, and AOS-based devices [9] but

also in spin-wave-based devices, an emergent research field called “magnonics” [10].

However, it is increasingly challenging to achieve low magnetic damping in metallic magnetic materials. The magnetic damping reflects the ability of the magnetization to precess around an effective magnetic field. Dissipation occurs due to interactions with the environment, the precession amplitude decreases, and the oscillating magnetization aligns again with the effective field. This damping process is characterized by the phenomenological Gilbert damping coefficient α within the Landau-Lifshitz-Gilbert formalism [11–14]. For many emerging spintronic and magnonic applications, this is particularly important in low-power applications that exploit magnetic dynamics such as STT switching, where the switching current is directly proportional to α [15]. This is also true for SOT devices, where a precessing magnetization generates a charge current in a metal and vice versa [9,16].

While low damping parameters are often obtained in ferrimagnetic insulating oxides such as yttrium iron garnet, where $\alpha = 7.35 \times 10^{-5}$ can be observed in the bulk [17], magnetic metals typically have much higher damping, where Fe-V alloys having a damping coefficient of around 2×10^{-3} [18,19] were considered state of the art for a thin film. Recently there was progress in obtaining a damping coefficient α as low as 2.1×10^{-3} in Fe-Co alloys [20]. However, there is a broader class of materials where ultralow magnetic damping in metallic magnets emerges

*stephane.andrieu@univ-lorraine.fr

as half-metal magnetic (HMM) behavior. Such materials emerged in 1983 when de Groot *et al.* [21] reported predictions of peculiar electronic properties of the NiMnSb half Heusler compound. Its electronic band structure was predicted to be in between that of a metal and an insulator. For the majority spin, responsible for the macroscopic magnetization, this material is a metal since electronic states are available around the Fermi energy (E_F). However, for minority spins, there is a gap around the Fermi energy. This peculiar property was called “half-metallic magnetic behavior.” NiMnSb is thus a metal for majority spins, whereas it is an insulator (at 0 K) for minority spins. Such properties lead to a full spin polarization at the Fermi energy, making this material an excellent candidate for spin-current generation. Furthermore, additional theoretical studies performed on HMM materials highlighted another physical property of major importance in spintronics: their magnetic damping coefficients were predicted to be extremely low compared with those of other conductive materials (a factor 100 below in the range from 10^{-5} to 10^{-4}) [22–24].

In HMM materials, extremely low magnetic damping coefficients are predicted for the following reason. The electronic band structure imposes no density of states (DOS) for minority spins. This spin-channel exchange is thus forbidden and leads to continuous precession [22]. In practice, other dissipation processes are possible, leading to a nonzero damping coefficient, but even when they are taken into account, damping coefficients as low as 10^{-5} are predicted [22,24]. The precession damping is thus much smaller in a HMM material than in a regular ferromagnetic material (with nonzero density of states at the Fermi energy for both spin channels). HMM materials are thus very promising materials for applications.

After the publication of the paper by de Groot *et al.* [21], HMM properties were theoretically predicted for many Heusler compounds [25–27]. However, it took a significant effort for experimentalists to obtain direct verification. Indeed, the direct evidence of a spin gap in the minority-spin channel was reported only very recently in Co_2MnSi [28,29]. On the other hand, as small magnetic damping coefficients were reported for several Heusler compounds, the measured values remained in the 10^{-3} range [30–35], which is at least 10 times larger than predicted and comparable with values in epitaxial Fe-V alloys [19], which are not HMM materials. In 2016, we measured for the first time a damping coefficient in the 10^{-4} range [29] (7×10^{-4} in Co_2MnSi , which was confirmed by another group in 2018 [36]). However, the fact that the magnetic damping values reported in the literature dedicated to HMM materials are often higher than 10^{-3} is puzzling. A recent theoretical study reported that the magnetic damping can vary strongly according to the chemical disorder in the unit cell [24]. Thus, one big challenge when one is growing X_2YZ full Heusler thin films is to be as

close as possible to the exact stoichiometry and achieve the chemically-ordered $L2_1$ phase as the outstanding properties of Co-based Heusler compounds are most often predicted for this $L2_1$ phase. However, Heusler alloys can crystallize in several phases with lower chemical ordering [37] without changing the atomic sites in the lattice. The most-encountered disordered phase is the B2 phase, where Y and Z atoms are randomly arranged with respect to each other, leading to a primitive unit cell instead of the fcc cell ($Fm\bar{3}m \rightarrow Pm\bar{3}m$). The extent to which the chemical disorder affects the physical properties is not clear. On one hand, *ab initio* calculations [24,38,39] and experiments [39,40] show that the physical properties (Curie temperature, cell parameter, magnetic moment, magnetic damping constant, and spin polarization at E_F) are not drastically different between the $L2_1$ phase and the B2 phase, and the half-metallic spin gap should be conserved. On the other hand, the correlation between the degree of chemical ordering and the physical properties suffers from a lack of experimental evidence since it is very difficult to manipulate the degree of chemical ordering without adding other parameters that need to be taken into account (such as introducing doping or reducing the crystallographic quality of the layer).

In this work, we present a systematic study of Co_2MnZ Heusler thin films epitaxially grown by molecular-beam epitaxy (MBE) with $Z = \text{Al, Si, Ga, Ge, Sn, Sb}$. The chemical ordering inside the Heusler fcc lattice is examined by *in situ* reflection high-energy electron diffraction (RHEED) and *ex situ* transmission electron microscopy (TEM). The spin polarization at the Fermi energy is determined by spin-resolved photoemission spectroscopy (SRPES) experiments performed with the CASSIOPEE beamline at the SOLEIL synchrotron facility. Finally, the damping coefficients are measured by ferromagnetic resonance (FMR) in a perpendicular geometry (dc magnetic field applied perpendicular to the film plane). Ultralow damping (in the range from 4×10^{-4} to 9×10^{-4}) is observed here for at least four of these six materials and is discussed according to the spin polarization determined experimentally and compared with theoretical predictions.

II. EXPERIMENTAL RESULTS

A. Sample growth and structural characterization

All the films are grown by molecular-beam epitaxy. The stoichiometry of the Heusler films is accurately controlled by use of quartz microbalances (see Appendix A). *In situ* RHEED performed all along the growth process allows us to control the epitaxy process and the chemical ordering in the Heusler unit cell. If chemical ordering occurs, additional RHEED streaks should be observed along the Heusler [110] azimuth compared with the A2 or B2 phase [41]. Typical RHEED patterns obtained after the growth process as well as the corresponding STEM high-angle

annular-dark-field (HAADF) images are shown in Fig. 1. All the films show additional streaks along $[110]$ RHEED patterns and the STEM HAADF images show the correct positioning of the Z element, meaning that the film structure is compatible with the L_{21} structure, except for Co_2MnAl , which has a B2 structure, as reported in the literature [30].

B. Spin polarization

Since SRPES is a surface technique, the films are grown in a MBE chamber coupled to the synchrotron beamline (see Appendix B and Refs. [29,42]). The PES for each spin channel and the resulting SP are shown in Fig. 2 for the

Co_2MnZ series studied here. The results are discussed as a function of the Z element with the semiconductor terminology type III, IV, and V, and for simplicity we denote the different Heusler compounds as $\text{Co}_2\text{MnZ}_{\text{type}}$.

For the $\text{Co}_2\text{MnZ}_{\text{IV}}$ compounds ($Z = \text{Si}, \text{Ge}, \text{Sn}$) the SRPES spectra show a similar PES shape, which is expected because of the constant number of valence electrons in each compound. Importantly, they manifest the same transitions as depicted in our previous paper on Co_2MnSi [29], where two features are explained. First, the loss of spin polarization at E_F is caused by the presence of polarized surface states split by exchange coupling (denoted S_1 for majority spins and S_2 for minority spins in Fig. 2). These S_1 and S_2 transitions completely disappear

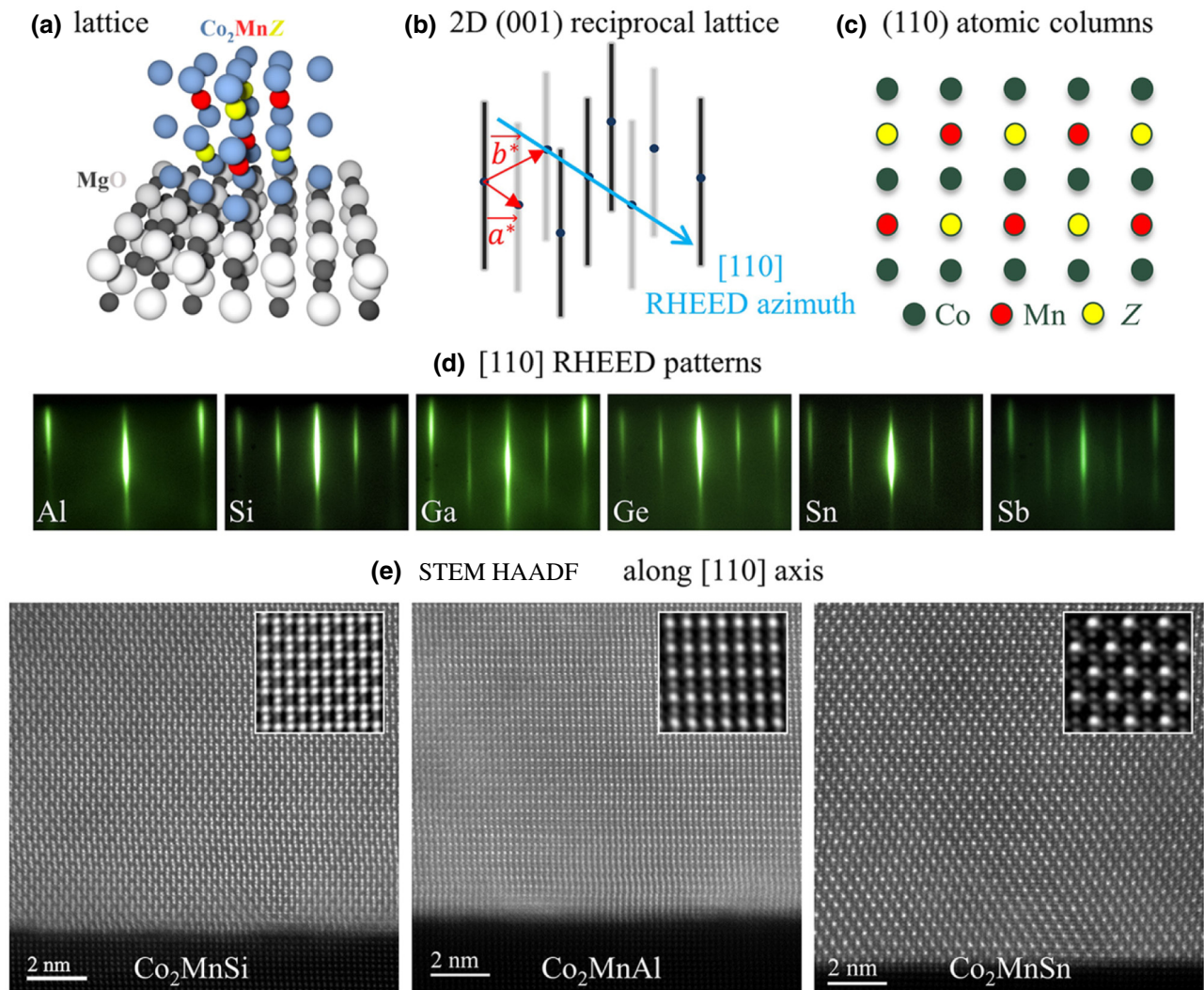


FIG. 1. (a) The epitaxial relationship between Co_2MnZ films and the MgO substrate. (b) Co_2MnZ (001) reciprocal lattice explored by electron diffraction (RHEED). (c) Atomic columns along the $[110]$ azimuth for the L_{21} ordering. (d) RHEED patterns along $[110]$ for the Co_2MnZ series. (e) STEM HAADF micrographs along the $[110]$ zone axis for the Co_2MnSi , Co_2MnAl , and Co_2MnSn films (enlargements in the insets). Note the small weight of Si (14 electrons) compared with Sn (50 electrons). The Z atoms are at the correct position in the cell as confirmed by RHEED and TEM, except for Co_2MnAl , where a mixing of Mn and Si is observed, leading to a B2 structure (no half streaks on the RHEED pattern and no contrast between the Mn and Z columns by microscopy). 2D, two-dimensional.

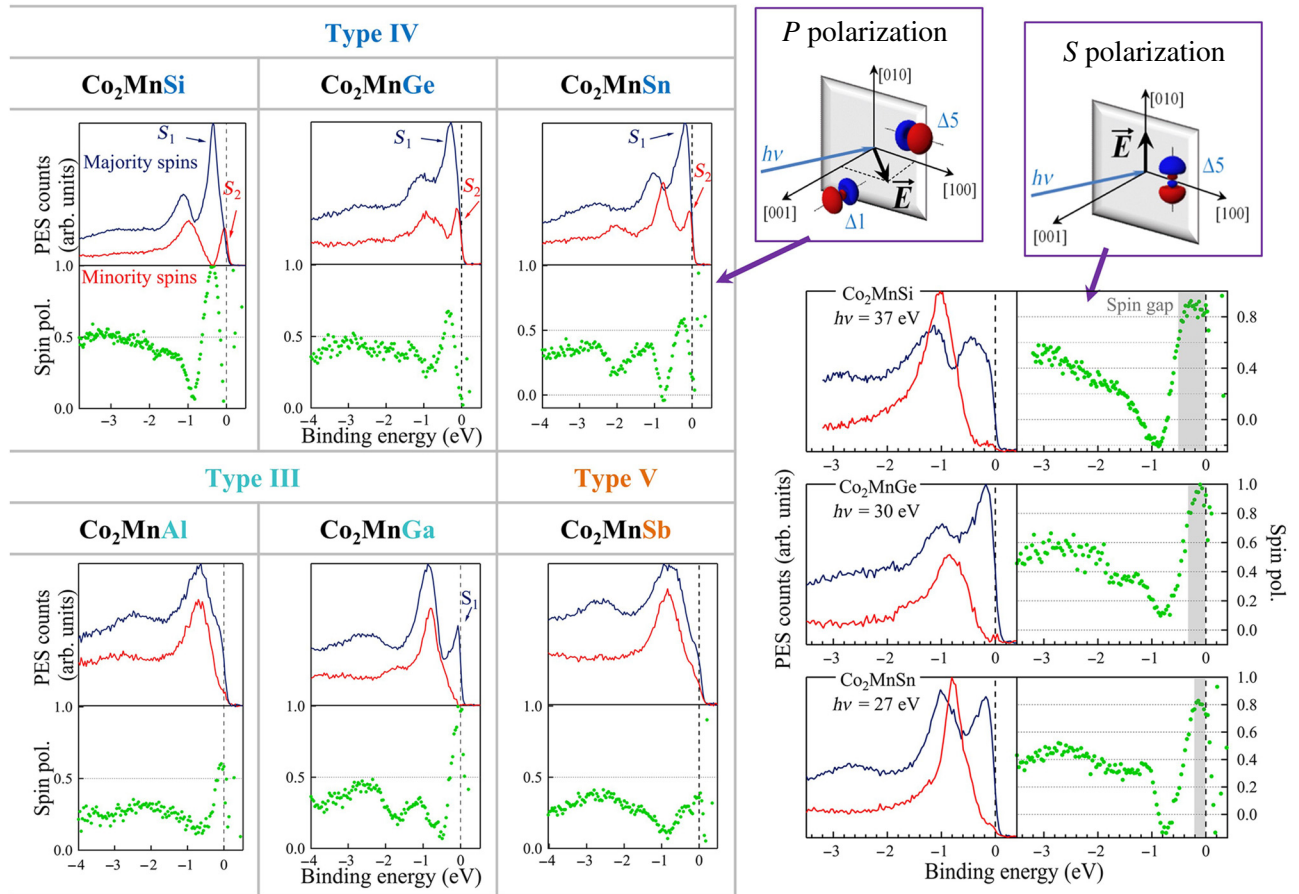


FIG. 2. Spin-resolved photoemission spectra measured for the Co_2MnZ series. Incoming photon energy of 37 eV is used for $Z = \text{Si}$, Al, Ga, and Sb, 30 eV is used for $Z = \text{Ge}$, and 27 eV is used for $Z = \text{Sn}$. We change the incoming photon energy because of surface states, resonant in photon energy, which depends on the Z element in the compound. The left graphs are obtained with p photon polarization. Surface transitions are observed and denoted as S_1 (majority-spin channel) and S_2 (minority-spin channel). S_1 and S_2 are responsible for the loss of spin polarization at E_F (see the text). Spin gaps are observed for Co_2MnGa and Co_2MnSi . The right graphs are obtained with s polarization of the photons on $\text{Co}_2\text{MnSi}(001)$, $\text{Co}_2\text{MnGe}(001)$, and $\text{Co}_2\text{MnSn}(001)$. The S_1 and S_2 transitions coming from surface states are now forbidden, leading to clear observation of the minority-spin gap.

when the surface is covered by an atomic layer, and high spin polarization is thus observed up to the Fermi energy (we studied MgO, Mn, and MnSi in Ref. [29]). These surface states are resonant with the photon energy [29], so they are observed only in the photon energy range from 25 to 45 eV depending on the compound (and were not observed in Ref. [28]). We observe exactly the same behavior for Ge and Sn. However, there is a significant difference between Co_2MnSi when compared with Co_2MnGe and Co_2MnSn . The minority-spin gap is large in Co_2MnSi , whereas it decreases in Co_2MnGe and Co_2MnSn . So the beginning of the spin gap is observed in Co_2MnSi (around -0.4 eV) despite the surface-state contribution around E_F , but this is no longer the case for Ge and Sn. In other words, the PES experiments including the surface states do not allow one to obtain the bulk spin polarization. To access it, one can change the photon polarization from p to s . We previously showed that the spin gap can thus be

observed up to E_F in Co_2MnSi [29]. We consequently perform the same experiment on Co_2MnGe and Co_2MnSn . The results are shown in Fig. 2. As in Co_2MnSi with use of s photon polarization, the suppression of the transitions coming from the surface states allows us to see the spin gap in Co_2MnGe , but more interestingly, a full spin polarization is now observed, confirming Co_2MnGe is HMM. The (pseudo)-spin-gap is also observed for Co_2MnSn . Even though the spin polarization is much larger than with p polarization in Fig. 2, this compound is not fully spin polarized and has SP of 80%.

For $\text{Co}_2\text{MnZ}_{\text{III}}$ compounds, the number of valence electrons is lower than in type-IV compounds, so E_F should decrease. This is actually observed, and the former surface states are above E_F and not occupied, so the SP is maximum at E_F . Therefore, the maximum spin polarization visible in Fig. 2 for the $\text{Co}_2\text{MnZ}_{\text{III}}$ compounds nearly corresponds to the beginning of the minority-spin gap. The

SP is observed to be close to 60% for Co_2MnAl , whereas full SP was obtained for Co_2MnGa .

For Co_2MnSb (a type-V compound), a quite small SP is observed (around 35%) but one important feature has to be taken into account. Sb is well known to strongly segregate during MBE growth [43]. This segregation was also observed in Sb-based Heusler compounds such as NiMnSb [44] and Co_2TiSb [45]. We directly observe this segregation using Auger spectroscopy. Since PES is a surface technique, the electronic properties of such a Sb-enriched surface are included with the underneath- Co_2MnSb PES contribution and may significantly affect the measured SP.

C. Magnetic damping measurements

The magnetic damping properties of these films are extracted from FMR measurements performed on the samples grown by MBE available at CASSIOPEE beamline facility (after they have been capped with Au) and also on samples grown by MBE at Institut Jean Lamour. The FMR

experiment allows one to study the precession dynamics of the electronic magnetic moment [11–14,46,47] in ferromagnetic materials (see Appendix C for details). Typical vector-network-analyzer FMR measurements performed on Co_2MnGe and Co_2MnSi are shown in Fig. 3. Figure 3(a) corresponds to the S_{11} reflection coefficient [48] for magnetic flux density of 1.9 and 2.38 T, respectively. For each field value, the real and imaginary parts of the dynamic susceptibility are fitted simultaneously (i.e., with use of the same parameters to enhance the fitting reliability) to extract the position of the resonance-frequency peak [Fig. 3(b)] and its half width at half maximum [Fig. 3(c)]. At $f=0$, the curve crosses the axis at $H = M_{\text{eff}} \approx M_S$ for small magnetic anisotropy, which is the case in these layers [49,50]. The measured effective magnetic moments per formula unit (f.u.) are reported in Table I for the whole Co_2MnZ series and are compared with theoretical values. Our experimental results tend to follow the $M_S = \Lambda - 24 \mu_B/\text{f.u.}$ Slater-Pauling rules [54], where Λ is the total number of valence electrons in the Heusler structure. Finally, the linewidth slopes in Fig. 3(c) give damping

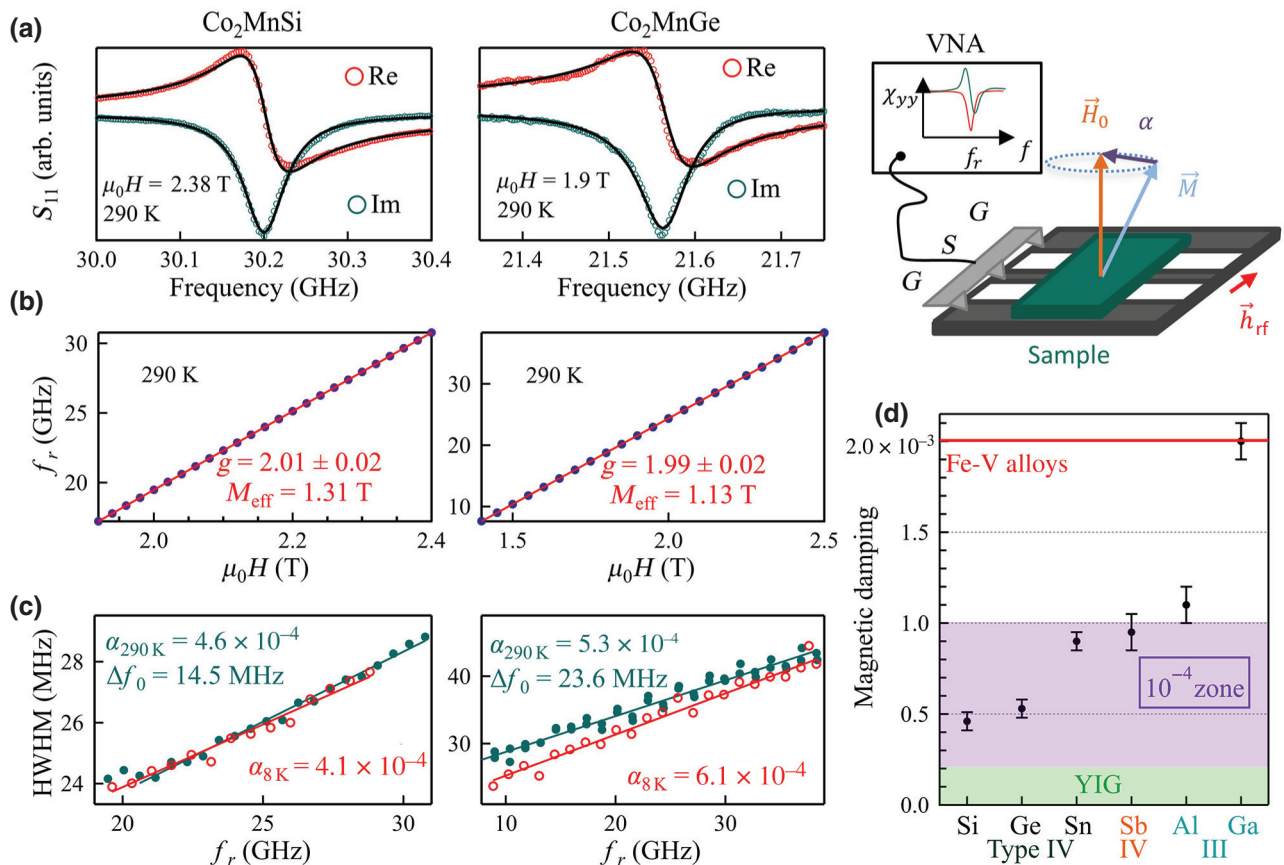


FIG. 3. Perpendicular FMR on Co_2MnGe and Co_2MnSi : (a) S_{11} parameter of the scattering matrix, (b) dependence of the FMR on the field, and (c) evolution of the linewidth versus FMR. (d) Measured damping for the Co_2MnZ series. The magnetic damping obtained in thin films of conductive Fe-V alloys and bulk insulating yttrium iron garnet (YIG) with our setup are shown as a comparison. The figure in the upper right corner is a schematic of our experimental FMR configuration. G, ground; HWHM, half width at half maximum; S, signal; VNA, vector network analyzer.

TABLE I. Experimental results obtained by FMR and SRPES and comparison with available theoretical results.

Z	Our experiments (290 K)						Theory (0 K)			
	a (Å)	M_{eff} ($\mu_B/\text{f.u.}$)	α	MaximumSP (%)	M_S ($\mu_B/\text{f.u.}$)	α	SP	Δ_{gap} (eV)	$E_F - E_{\text{VB}}$ (eV)	
Type III	Al	5.76	4.4	1.1×10^{-3} (290 K)	60	4.3 [38]	...	0.68 [51]	0.66 [51]	0 [52]
				1.15×10^{-3} (30 K)						
	Ga	5.77	5.4	2×10^{-3} (290 K)	100	4.09 [53]	...	0.67 [51]	0.3 [51]	0 [52]
				1.8×10^{-3} (30 K)						
Type IV	Si	5.65	5.1	4.6×10^{-4} (290 K)	100	4.94 [54]	6×10^{-5}	100	0.41 [24]	~ 0.2 [24]
				4.1×10^{-4} (8 K)						
	Ge	5.75	5	5.3×10^{-4} (290 K)	100	4.94 [54]	1.9×10^{-4}	100	0.58 [52]	0.81 [55]
				6.1×10^{-4} (8 K)						
	Sn	6.00	5.6	9×10^{-4} (290 K)	81	4.98 [54]	7×10^{-4}	0.77 [51]	0.54 [56]	0.03 [56]
				10^{-3} (8 K)						
Type V	Sb	5.96	5.1	9.6×10^{-4} (290 K)	36	6 [59]	...	100 [53]	0.41 [51]	0 [51]
									0.17 [52]	-0.06 [52]
									0.65 [59]	0.56 [59]
									0.33 [52]	0.39 [52]

coefficients of 5.3×10^{-4} for Co_2MnGe and 4.6×10^{-4} for Co_2MnSi at 290 K (6.1×10^{-4} and 4.1×10^{-4} at 8 K), the lowest of the Co_2MnZ series [Fig. 3(d)]. Moreover, the inhomogeneous linewidths Δf_0 in Co_2MnGe and Co_2MnSi (23.6 and 14.5 MHz, respectively) are very small, almost comparable with those of bulk magnetic insulators such as yttrium iron garnet. Such small values imply excellent homogeneity of the magnetic properties (hence a high crystal quality) in our films. Finally, one should note that this kind of FMR measurement leads to an effective value of the damping larger than the intrinsic value for the material [20,56,60]. Indeed, the effective damping measured here has extrinsic contributions, such as radiative-damping, eddy-current-damping, and spin-pumping contributions. Thus, the magnetic damping coefficients reported in Table I include these extrinsic contributions and correspond to an upper limit of the true values. Recently, Shaw *et al.* [35] demonstrated a method to remove the extrinsic damping contributions in FMR measurements and obtain a better estimate of the true magnetic damping in Co_2MnGe (measured damping 1.5×10^{-3} , which becomes smaller than 10^{-3} after corrections). Thus, the theoretical values are likely found to be lower than experimental ones without correction as reported here. Even with these extrinsic contributions, the measured damping coefficients of the whole Co_2MnZ series are in the ultralow damping range (four of six in the 10^{-4} range and two below 2×10^{-3}), in agreement with theoretical predictions.

III. DISCUSSION

All the experimental results obtained in this work are reported in Table I, together with theoretical predictions found in the literature. Looking first the PES results obtained for $\text{Co}_2\text{MnZ}_{\text{IV}}$ compounds, the observed full spin polarization for Si and Ge is consistent with theoretical calculations regarding the calculated width of the spin

gap and the position of the Fermi energy in the middle of the gap. For calculations of the Co_2MnSi band structure, the Fermi energy is located in the middle of the spin gap [24,55] and a large gap is obtained (0.8 eV [55], 0.41 eV [24,52]). Our results are consistent with these theoretical predictions since the measured (half) gap between the minority-spin valence band and E_F is around 0.4 eV (Fig. 2). In the case of Co_2MnGe , the calculated gap is smaller (0.58 eV [51]) and E_F is closer to the minority-spin valence band, again consistent with our observations (half gap around 0.25 eV, see Fig. 2). Finally, with regard to calculations of Co_2MnSn bands, Kandpal *et al.* [51] found E_F to be in the gap and close to the valence band (so HMM), whereas Ishida *et al.* [52] found it to be 0.06 eV below the top valence band (so not HMM). Our results do not allow us to conclude about this point (HMM or not) since our measurements are broadened by temperature (300 K). However, both scenarios are consistent with the limited SP reported here. To summarize, the SRPES results for these type-IV Heusler compounds are well described by *ab initio* calculations. The presence of this minority-spin gap at the Fermi energy should reduce the magnetic damping due to the removal of one conduction channel responsible for scattering processes involving spin flip (in other words, it should decrease the energy dissipation through spin relaxation in the system). Our magnetic damping measurements are in agreement with this mechanism. Indeed, the larger the spin gap, the smaller the magnetic damping. These large spin gaps in Co_2MnSi and Co_2MnGe also explain why the magnetic damping is rather independent of the temperature for these two compounds (thermal-fluctuation energy lower than the spin gap even at room temperature). But our FMR results allow us to go further in the case of Co_2MnSn , since its very low magnetic damping strongly suggests that Co_2MnSn is a true HMM material as predicted by Kandpal *et al.* [51]. To conclude, our results highlight a clear correlation between the theoretical gap

width and the Fermi-energy position with the experimental SP and magnetic damping values.

With regard to band calculations on Co_2MnAl and Co_2MnGa (type-III compounds) considering the L_{21} phase, the theoretical SPs at E_F are 68% and 67%, respectively [51]. Full SP is not achieved because a small minority-spin DOS remains at the Fermi energy. Strictly speaking, these compounds are not predicted to be true HMM materials. However, this former DOS is so small that a strong SP is still calculated. To account for this peculiar behavior, theoreticians use the term “pseudo gap” [53]. The SRPES results shown in Fig. 2 for the B2-ordered Co_2MnAl are in good agreement with this theoretical prediction since a SP of 60% is obtained at E_F . It is also consistent with the theoretical work of Pradines *et al.* [24], explaining that the spin polarization at E_F should stay unchanged between the L_{21} chemical phase and the B2 chemical phase. However, the situation is different for Co_2MnGa . We observe full SP, in clear disagreement with theory. Our experimental results show that E_F is located in a true band gap, but very close to the minority-spin valence band. As a consequence, this leads to low magnetic damping (compared with regular ferromagnetic layers) but higher than in type-IV compounds due to the proximity of E_F to the valence band.

For Co_2MnSb , theoretical calculations lead to a large spin gap (0.65 eV), with E_F very close to the empty minority-spin conduction band (0.09 eV below) in Ref. [59] or even in the conduction band in Ref. [52]. The experimental results are puzzling. Our PES results are not consistent with a HMM behavior, but very low magnetic damping is, however, observed, consistent with a HMM behavior. The low SP can be explained by considering Sb segregation at the surface that does not affect the bulk SP. We conclude that Co_2MnSb is likely HMM in the bulk, but its magnetic damping is higher than for type-IV materials because of the proximity of E_F to the minority-spin conduction band. These observations finally point out that our SRPES analysis is useful to obtain bulk properties for (001) Co_2MnSi , Co_2MnGe , Co_2MnSn , Co_2MnGa , and Co_2MnAl but not for (001) Co_2MnSb .

IV. CONCLUSIONS

This work provides a clear experimental demonstration that the unique electronic band structure of half-metal magnetic materials leads to ultralow magnetic damping. This study allows us to determine several key points to achieve ultralow damping. The most-important ingredients are a large minority-spin band gap and a suitable position of the Fermi energy in the band gap that is not too close to the minority-spin valence and conduction bands. To achieve this behavior requires growth of high-quality crystalline films with control of the stoichiometry. The measured magnetic damping coefficients of the series

match qualitatively with the spin polarization at E_F predicted by the theoretical calculations and the SP measured by SRPES without surface states. First, Co_2MnSi and Co_2MnGe have Fermi energy inside a large half-metallic gap and have ultralow magnetic damping coefficients below 6×10^{-4} (although the intrinsic damping will be even lower). Second, Co_2MnSn and Co_2MnSb , with Fermi energy very close to a minority-spin band (valence band for the former, conduction band for the latter), have intermediate magnetic damping coefficients ($6 \times 10^{-4} \leq \alpha \leq 10^{-3}$). Third, Co_2MnAl and Co_2MnGa are not predicted to be pure HMM materials and their damping coefficients are found to be above those of the rest of the series, being $10^{-3} \leq \alpha \leq 2 \times 10^{-3}$. Nevertheless, the case of Co_2MnGa is puzzling since we observe full spin polarization, whereas the magnetic damping coefficient is the highest in the series. Finally, the ultralow magnetic damping we obtain in Co_2MnSi (4.1×10^{-4}) and Co_2MnGe (5.3×10^{-4}) has never been observed in a conductive material. One should note that in devices usually grown by sputtering, the crystalline quality is not as good as in epitaxial films. However, the spin gap is predicted in the whole Brillouin zone so there is no fundamental reason to not obtain ultraslow damping in sputtered Heusler-based devices. Such ability to obtain easy precession of the magnetization offers extraordinary opportunities for fabrication of more-efficient spintronic devices, such as spin-torque-FMR, spin-pumping FMR, optical switching, or magnonic-based devices.

ACKNOWLEDGMENTS

This work was supported partly by the french PIA project “Lorraine Université d’Excellence”, Reference No. ANR-15-IDEX-04-LUE, and by the Agence Nationale de la Recherche (France) under contract No. ANR-17-CE24-0008 (CHIPMuNCS). Some UHV experiments were performed with equipment from the TUBE—DauvM funded by FEDER (EU), ANR, the Region Lorraine and Grand Nancy. We acknowledge Eric E. Fullerton from the Center for Memory and Recording Research (University of California, San Diego, USA) for his critical reading of the manuscript.

APPENDIX A: SAMPLE GROWTH AND STRUCTURAL CHARACTERIZATION

The substrate used to obtain single-crystal Heusler films is $\text{MgO}(001)$ due to the small misfit between MgO and Co_2MnZ layers considered here. All the films are grown by molecular-Beam epitaxy. Co, Si, and Ge are evaporated with use of electron guns, whereas Mn, Al, Ga, Sn, and Sb are evaporated by use of Knudsen cells. Epitaxial films are obtained directly on MgO for $Z = \text{Al, Si, Ga, and Ge}$. As this process is not successful with $Z = \text{Sb}$, $\text{Co}_2\text{MnSb}(001)$ films are obtained on a 10-nm $\text{V}(001)$

buffer layer grown on MgO. The Heusler films are all 20 nm thick. The starting temperature for the growth is fixed to 450 °C (measured by a thermocouple beside the sample holder) and the Heusler films are heated to 750 °C after the growth to improve the chemical ordering in the lattice and the surface quality. Auger spectroscopy is systematically performed after the growth process and allows us to verify that no surface contamination occurs (no O and C detected). The stoichiometry is a crucial point to get the best electronic and magnetic properties of these compounds. For this purpose, the fluxes of each element are calibrated with use of a quartz microbalance located at the sample's location. The flux variations during the process are observed to be below 2%. To achieve good stoichiometry, the Co flux is fixed to 2×10^{14} at./cm² s and the Mn and Z element fluxes are fixed to 10^{14} at./cm² s. Considering these fluxes and a sticking coefficient on quartz equal to 1 for all these materials, the time to complete a layer is expected to be 3.0 s for Co₂MnSi. We measure exactly this completion time by using RHEED intensity oscillations performed during the growth. Moreover, the desired total thickness of the films (fixed by use of the fluxes and the growth duration) is in perfect agreement with the final thickness determined by XRD reflectivity measurements. RHEED performed all along the growth process also allows us to verify that the Heusler lattice grows with the epitaxial relationship MgO [100] (001) // Co₂MnZ [110] (001), meaning that the Heusler single crystal is turned by 45° compared with the MgO lattice as shown in Fig. 1. As RHEED provides information only about the surface, θ -2 θ XRD experiments are performed *ex situ*. All the films show (111) peaks by XRD, meaning that the film structure is compatible with the L2₁ structure, except for Co₂MnAl, for which no (111) peak is observed which is compatible with the B2 structure, as reported in the literature [30]. Finally, STEM HAADF investigations were performed with a JEM-ARM200F cold-field-emission-gun transmission electron microscope or scanning transmission electron microscope operating at 200 kV and equipped with a spherical aberration (Cs) probe and image correctors (point resolution 0.12 nm in TEM mode and 0.078 nm in STEM mode).

APPENDIX B: SPIN-RESOLVED PHOTOEMISSION SPECTROSCOPY

SRPES experiments are performed with the CASIOPEE beamline at the SOLEIL synchrotron facility. The setup and analysis process are detailed in Ref. [42] (beamline description) and Ref. [29] (study of Co₂MnSi). The spin resolution is obtained with a Mott detector with an overall energy resolution of 150 meV in the photon energy range from 30 to 40 eV used in this study. As discussed in Ref. [29], our experimental conditions allow us to explore around 80% of the Brillouin zone according to

the photon energy range used in this study. As the magnetization of the films is always in plane in our samples, the films are first magnetized *in situ* before the photoemission measurement by application of an in-plane magnetic field of 200 Oe, which is sufficient to saturate the magnetization (the coercive fields in our samples are always below 100 Oe). As the SRPES measurement has to be performed without any magnetic field, the spin polarization extracted from raw PES spectra is obtained at remanence. The remanence is systematically measured on the same films *ex situ* after the samples have been capped with 5-nm-thick gold. The remanence is observed to range from 80% to 100% depending on the Co₂MnZ compound. The true spin polarizations shown in this paper are thus obtained by correcting the SRPES spectra from remanence.

APPENDIX C: MAGNETIC DAMPING MEASUREMENTS

As in NMR, the precession occurs when an oscillating magnetic field of small amplitude is generated perpendicular to the magnetic moment equilibrium, which corresponds, in a ferromagnet, to the magnetization direction. This equilibrium position is imposed by the effective field derived from the magnetic free-energy density, which includes exchange, dipolar-interaction, and magnetocrystalline-anisotropy energies. The magnetic damping is, by definition, inversely related to the lifetime of the precession. The damping coefficient is thus extracted by our looking at the linewidth of the resonance peak in the frequency regime. The larger the linewidth, the higher the damping and the shorter the precession motion. FMR experiments are performed in the *perpendicular geometry*, where the static magnetic field is applied out of the plane of the film to avoid extrinsic broadening of the linewidth due to the two-magnon scattering [46,47]. The rf magnetic field is generated, by a vector network analyzer, in a coplanar waveguide (ground-signal-ground geometry), on top of which the sample is placed face down. Measurements are performed in reflection geometry. The physical parameter extracted from these experiments is the S_{11} coefficient of the scattering matrix of the line, from which the dynamic susceptibility of the magnetic layer is extracted [47]. In the case of a perpendicular geometry, the Kittel law [11] [Eq. (C1)] becomes linear and so does the evolution of the peak's linewidth versus its own resonance frequency. The slope of this curve is directly the magnetic damping coefficient [(Eq. (C2))]:

$$f_r = \gamma_0(H - M_S + H_{k\perp}) = \gamma_0(H - M_{\text{eff}}), \quad (\text{C1})$$

$$\Delta f = 2\alpha\gamma_0(H - M_{\text{eff}}) + 2\Delta f_0 = 2\alpha f_r + 2\Delta f_0, \quad (\text{C2})$$

where f_r refers to the resonance frequency, γ_0 the gyro-magnetic ratio of the electron, H is the magnetic field strength, M_S is the magnetization, $H_{k\perp}$ is the perpendicular

magnetic anisotropy, the effective magnetization $M_{\text{eff}} = M_S - H_{k\perp}$, Δf is the full width at half maximum, Δf_0 is the inhomogeneous half linewidth, and α is the Gilbert magnetic damping coefficient. The shift in frequency of the resonance peak versus the field is imposed by the gyromagnetic ratio γ_0 of the electron, which should be 28 GHz/T in the case of a pure delocalized ferromagnetic model (free-electron model). However, in a solid, this ratio can be different mainly due to spin-orbit coupling since γ_0 is proportional to the Landé g factor. The fitted slopes in Fig. 3(c) give $\gamma_0 = 27.9$ and 28.2 GHz/T, corresponding to a Landé g factor of 1.99 and 2.01 (very close to the noninteracting-electron case, as expected for 3d compounds).

-
- [1] W. H. Butler, X.-G. Zhang, T. C. Schulthess, and J. M. MacLaren, Spin-dependent tunneling conductance of Fe[MgO]Fe sandwiches, *Phys. Rev. B* **63**, 054416 (2001).
- [2] J. Mathon and A. Umerski, Theory of tunneling magnetoresistance of an epitaxial Fe/MgO/Fe(001) junction, *Phys. Rev. B* **63**, 220403(R) (2001).
- [3] J. C. Slonczewski, Conductance and exchange coupling of two ferromagnets separated by a tunneling barrier, *J. Magn. Mater.* **159**, L1 (1996).
- [4] L. Berger, Emission of spin waves by a magnetic multilayer traversed by a current, *Phys. Rev. B* **54**, 9353 (1996).
- [5] I. M. Miron, K. Gatello, G. Gaudin, P.-J. Zermatten, M. V. Costache, S. Auffret, S. Bandiera, B. Rodmacq, A. Schuhl, and P. Gambardella, Perpendicular switching of a single ferromagnetic layer induced by in-plane current injection, *Nature* **476**, 189 (2011).
- [6] C.-H. Lambert, S. Mangin, B. S. D. Ch, S. Varaprasad Y, K. Takahashi, M. Hehn, M. Cinchetti, G. Malinowski, K. Hono, Y. Fainman, M. Aeschlimann, and E. E. Fullerton, All-optical control of ferromagnetic thin films and nanostructures, *Science* **345**, 1337 (2014).
- [7] J.-C. Rojas-Sánchez, N. Reyren, P. Laczkowski, W. Savero, J.-P. Attané, C. Deranlot, M. Jamet, J.-M. George, L. Vila, and H. Jaffrès, Spin Pumping and Inverse Spin Hall Effect in Platinum: The Essential Role of Spin-Memory Loss at Metallic Interfaces, *Phys. Rev. Lett.* **112**, 106602 (2014).
- [8] F. Hellman, A. Hoffman, Y. Tserkovnyak, G. S. D. Beach, E. E. Fullerton, C. Leighton, A. H. MacDonald, D. C. Ralph, D. A. Arena, *et al.*, Interface-induced phenomena in magnetism, *Rev. Mod. Phys.* **89**, 025006 (2017).
- [9] I. L. Prejbeanu, S. Bandiera, J. Alvarez-Héroult, R. C. Sousa, B. Dieny, and J.-P. Nozières, Thermally assisted MRAMs: ultimate scalability and logic functionalities, *J. Phys. D: Appl. Phys.* **46**, 074002 (2013).
- [10] A. V. Chumak and H. Schultheiss, Magnonics: spin waves connecting charges, spins and photons, *J. Phys. D: Appl. Phys.* **50**, 300201 (2017).
- [11] C. Kittel, On the theory of ferromagnetic resonance absorption, *Phys. Rev.* **73**, 155 (1948).
- [12] H. Suhl, Theory of the magnetic damping constant, *IEEE Trans. Magn.* **34**, 1834 (1998).
- [13] V. Kamberský, Spin-orbital Gilbert damping in common magnetic metals, *Phys. Rev. B* **76**, 134416 (2007).
- [14] K. Gilmore, Y. U. Idzerda, and M. D. Stiles, Identification of the Dominant Precession-Damping Mechanism in Fe, Co, and Ni by First-Principles Calculations, *Phys. Rev. Lett.* **99**, 027204 (2007).
- [15] D. C. Ralph and M. D. Stiles, Spin transfer torques, *J. Mag. Mag. Mat.* **320**, 1190 (2008).
- [16] K.-S. Lee, S.-W. Lee, B.-C. Min, and K.-J. Lee, Threshold current for switching of a perpendicular magnetic layer induced by spin Hall effect, *Appl. Phys. Lett.* **102**, 112410 (2013).
- [17] C. Hauser, T. Richter, N. Homonnay, C. Eisenschmidt, M. Qaid, H. Deniz, D. Hesse, M. Sawicki, S. G. Ebbinghaus, and G. Schmidt, Yttrium iron garnet thin films with very low damping obtained by recrystallization of amorphous material, *Sci. Rep.* **6**, 20827 (2016).
- [18] C. Scheck, L. Cheng, I. Barsukov, Z. Frait, and W. E. Bailey, Low Relaxation Rate in Epitaxial Vanadium-Doped Ultrathin Iron Films, *Phys. Rev. Lett.* **98**, 117601 (2007).
- [19] T. Devolder, M. Manfrini, T. Hauet, and S. Andrieu, Compositional dependence of the magnetic properties of epitaxial FeV/MgO thin films, *Appl. Phys. Lett.* **103**, 242410 (2013).
- [20] M. A. W. Schoen, D. Thonig, M. L. Schneider, T. J. Silva, H. T. Nembach, O. Eriksson, O. Karis, and J. M. Shaw, Ultra-low magnetic damping of a metallic ferromagnet, *Nat. Phys.* **12**, 839 (2016).
- [21] R. A. de Groot, F. M. Mueller, P. G. van Engen, and K. H. J. Buschow, New Class of Materials: Half-Metallic Ferromagnets, *Phys. Rev. Lett.* **50**, 2024 (1983).
- [22] C. Liu, C. K. A. Mewes, M. Chshiev, T. Mewes, and W. H. Butler, Origin of low Gilbert damping in half metals, *Appl. Phys. Lett.* **95**, 022509 (2009).
- [23] B. Pigeau, G. de Loubens, O. Klein, A. Riegler, F. Lochner, G. Schmidt, L. W. Molenkamp, V. S. Tiberkevich, and A. N. Slavin, Frequency-controlled magnetic vortex memory, *Appl. Phys. Lett.* **96**, 132506 (2010).
- [24] B. Pradines, R. Arras, I. Abdallah, N. Biziere, and L. Calmels, First-principles calculation of the effects of partial alloy disorder on the static and dynamic magnetic properties of Co₂MnSi, *Phys. Rev. B* **95**, 094425 (2017).
- [25] I. Galanakis and P. Mavropoulos, Spin-polarization and electronic properties of half-metallic Heusler alloys calculated from first principles, *J. Phys.: Condens. Matter* **19**, 315213 (2007).
- [26] I. Kastnelson, V. Yu. Irkhin, L. Chioncel, A. I. Lichtenstein, and R. A. de Groot, Half-metallic ferromagnets: from band structure to many-body effects, *Rev. Mod. Phys.* **80**, 315 (2008).
- [27] T. Graf, C. Felser, and S. S. P. Parkin, Simple rules for the understanding of Heusler compounds, *Prog. Solid State Ch.* **39**, 1 (2011).
- [28] M. Jourdan, J. Minar, J. Braun, A. Kronenberg, S. Chadov, B. Balke, A. Gloskovskii, M. Kolbe, H. J. Elmers, G. Schonhense, H. Ebert, C. Felser, and M. Klau, Direct observation of half-metallicity in the Heusler compound Co₂MnSi, *Nat. Commun.* **5**, 3974 (2014).
- [29] S. Andrieu, A. Neggache, T. Hauet, T. Devolder, A. Hallal, M. Chshiev, A. M. Bataille, P. Le Fèvre, and F. Bertran, Direct evidence for minority spin gap in the Co₂MnSi Heusler compound, *Phys. Rev. B* **93**, 094417 (2016).

- [30] S. Trudel, O. Gaier, J. Hamrle, and B. Hillebrands, Magnetic anisotropy, exchange and damping in cobalt-based full-Heusler compounds: An experimental review, *J. Phys. D: Appl. Phys.* **43**, 19 (2010).
- [31] M. Oogane, T. Kubota, H. Naganuma, and Y. Ando, Magnetic damping constant in Co-based full Heusler alloy epitaxial films, *J. Phys. D: Appl. Phys.* **48**, 164012 (2015).
- [32] S. Husain, S. Akansel, A. Kumar, P. Svedlindh, and S. Chaudhary, Growth of Co₂FeAl Heusler alloy thin films on Si(100) having very small Gilbert damping by Ion beam sputtering, *Sci. Rep.* **6**, 28692 (2016).
- [33] I. Abdallah, B. Pradines, N. Ratel-Ramond, G. Benassayag, R. Arras, L. Calmels, J.-F. Bobo, E. Snoeck, and N. Biziere, Evolution of magnetic properties and damping coefficient of Co₂MnSi Heusler alloy with Mn/Si and Co/Mn atomic disorder, *J. Phys. D: Appl. Phys.* **50**, 035003 (2017).
- [34] L. Bainsla, R. Yilgin, M. Tsujikawa, K. Z. Suzuki, M. Shirai, and S. Mizukami, Low magnetic damping for equiatomic CoFeMnSi Heusler alloy, *J. Phys. D: Appl. Phys.* **51**, 495001 (2018).
- [35] J. M. Shaw, E. K. Delczeg-Czirjak, E. R. J. Edwards, Y. Kvashnin, D. Thonig, M. A. W. Schoen, M. Puffall, M. L. Schneider, T. J. Silva, O. Karis, K. P. Rice, O. Eriksson, and H. T. Nembach, Magnetic damping in sputter-deposited Co₂MnGe Heusler compounds with A₂, B₂, and L₂₁ orders: Experiment and theory, *Phys. Rev. B* **97**, 094420 (2018).
- [36] M. Oogane, A. P. McFadden, K. Fukuda, M. Tsunoda, Y. Ando, and C. J. Palmström, Low magnetic damping and large negative anisotropic magnetoresistance in half-metallic Co_{2-x}Mn_{1+x}Si Heusler alloy films grown by molecular beam epitaxy, *Appl. Phys. Lett.* **112**, 262407 (2018).
- [37] G. E. Bacon and J. S. Plant, Chemical ordering in Heusler alloys with the general formula A₂BC or ABC, *J. Phys. F: Metal. Phys.* **1**, 524 (1971).
- [38] X. Zhu, E. Jiang, Y. Dai, and C. Luo, Stability, magnetic, & electronic properties of L₂₁ and B₂ phases in Co₂MnAl Heusler alloy, *J. Alloys Compd.* **632**, 528 (2015).
- [39] A. Kumar, F. Pan, S. Husain, S. Akansel, R. Brucas, L. Bergqvist, S. Chaudhary, and P. Svedlindh, Temperature-dependent Gilbert damping of Co₂FeAl thin films with different degree of atomic order, *Phys. Rev. B* **96**, 224425 (2017).
- [40] A. Rajanikanth, D. Kande, Y. K. Takahashi, and K. Hono, High spin polarization in a two phase quaternary Heusler alloy Co₂MnAl_{1-x}Sn_x, *J. Appl. Phys.* **101**, 09J508 (2007).
- [41] A. Neggache, T. Hauet, F. Bertran, P. Le Le Fèvre, S. Petit-Watelot, T. Devolder, Ph. Ohresser, P. Boulet, C. Mewes, S. Maat, J. R. Childress, and S. Andrieu, Testing epitaxial Co_{1.5}Fe_{1.5}Ge electrodes in MgO-based MTJs, *Appl. Phys. Lett.* **104**, 252412 (2014).
- [42] S. Andrieu, L. Calmels, T. Hauet, F. Bonell, P. Le Fèvre, and F. Bertran, Spectroscopic & transport studies of Co_xFe_{1-x}/MgO based MTJs, *Phys. Rev. B* **90**, 214406 (2014).
- [43] S. Andrieu, Sb adsorption on Si(111) analyzed by ellipsometry and reflection high energy electron diffraction: Consequences for Sb doping in molecular beam epitaxy, *J. Appl. Phys.* **69**, 1366 (1991).
- [44] P. Turban, S. Andrieu, B. Kierren, E. Snoeck, C. Teodorescu, and A. Traverse, Growth and characterization of single crystalline NiMnSb thin films and epitaxial NiMnSb / MgO / NiMnSb(001) trilayers, *Phys. Rev. B* **65**, 134417 (2002).
- [45] J. K. Kawasaki, A. Sharan, L. I. M. Johansson, M. Hjort, R. Timm, B. Thiagarajan, B. D. Schultz, A. Mikkelsen, A. Janotti, and C. J. Palmström, A simple electron counting model for half-Heusler surfaces, *Sci. Adv.* **4**, eaar5832 (2018).
- [46] K. Lenz, H. Wende, W. Kuch, K. Baberscke, K. Nagy, and A. Jánossy, Two-magnon scattering and viscous Gilbert damping in ultrathin ferromagnets, *Phys. Rev. B* **73**, 144424 (2006).
- [47] K. Zakeri, J. Lindner, I. Barsukov, R. Meckenstock, M. Farle, U. von Hörsten, H. Wende, W. Keune, J. Røcker, *et al.*, Spin dynamics in ferromagnets: Gilbert damping and two-magnon scattering, *Phys. Rev. B* **76**, 104416 (2007).
- [48] C. Bilzer, T. Devolder, Joo-Von Kim, G. Council, C. Chappert, S. Cardoso, and P. P. Freitas, Study of the dynamic magnetic properties of soft CoFeB films, *J. Appl. Phys.* **100**, 053903 (2006).
- [49] Yu. V. Goryunov, N. N. Garif'yanov, G. G. Khaliullin, I. A. Garifullin, L. R. Tagirov, F. Schreiber, Th. Mühge, and H. Zabel, Magnetic anisotropies of sputtered Fe films on MgO substrates, *Phys. Rev. B* **52**, 13450 (1995).
- [50] A. Butera, J. L. Weston, and J. A. Barnard, Ferromagnetic resonance of epitaxial Fe₈₁Ga₁₉(110) thin films, *J. Mag. Mag. Mat.* **284**, 17 (2004).
- [51] H. C. Kandpal, G. H. Fecher, and C. Felser, Calculated electronic and magnetic properties of the half-metallic, transition metal based Heusler compounds, *J. Phys. D: Appl. Phys.* **40**, 1507 (2007).
- [52] S. Ishida, S. Fujii, S. Kashiwagi, and S. Asano, Search for half-metallic Heusler compounds in Co₂MnZ (Z=IIIb, IVb, Vb element), *J. Phys. Soc. Jpn.* **64**, 2152 (1995).
- [53] K. Özdoğan, E. Şaşıoğlu, B. Aktaş, and I. Galanakis, Doping and disorder in the Co₂MnAl and Co₂MnGa half-metallic Heusler alloys, *Phys. Rev. B* **74**, 172412 (2006).
- [54] I. Galanakis, P. H. Dederichs, and N. Papanikolaou, Slater-Pauling behavior and origin of the half-metallicity of the full-Heusler alloys, *Phys. Rev. B* **66**, 174429 (2002).
- [55] S. Picozzi, A. Continenza, and A. J. Freeman, Co₂MnX (X=Si, Ge, Sn) Heusler compounds: An ab initio study of their structural, electronic, and magnetic properties at zero and elevated pressure, *Phys. Rev. B* **66**, 094421 (2002).
- [56] Y. Li and W. E. Bailey, Wave-Number-Dependent Gilbert Damping in Metallic Ferromagnets, *Phys. Rev. Lett.* **116**, 117602 (2016).
- [57] S. Ouardi, Ph.D Thesis, Johannes Gutenberg-University at Mainz, 2012.
- [58] A. Pradines, R. Arras, and L. Calmels, Effects of partial B₂, D₀₃ and A₂ disorders on the magnetic properties of the Heusler alloys Co₂FeAl, Co₂MnSn and Co₂MnAl for spintronic applications, in preparation.
- [59] H. M. Huang, S. J. Luo, and K. L. Yao, First-principles investigation of the electronic structure and magnetism of Heusler alloys CoMnSb and Co₂MnSb, *Physica B* **406**, 1368 (2011).
- [60] M. A. W. Schoen, J. M. Shaw, H. T. Nembach, M. Weiler, and T. J. Silva, Radiative damping in waveguide-based ferromagnetic resonance measured via analysis of perpendicular standing spin waves in sputtered permalloy film, *Phys. Rev. B* **92**, 184417 (2015).